STM JOURNALS

Journal of
Polymer & Composites

ISSN: 2321-2810 (Online)
ISSN: 2321-8525 (Print)
Volume 14, Special Issue 3, 2026
DOI (Journal): 10.37591/JoPC

https://journals.stmjournals.com/jopc

Research JoPC

Fabrication and Comparative Study of Synthetic and Eggshell Waste Derived Hydroxyapatite-Based Composites for Biomedical Applications

Subhasis Nath[1], Sujan Krishna Samanta[2], Sourav Debnath[3,*], Soumya Mukherjee[4]

Abstract

Hydroxyapatite is widely used as a bioceramic material in orthopedic and dental field because of its exceptional biocompatibility and bioactivity. Hydroxyapatite (HAp) doped with several mineral ions has been frequently reported to further enhance its bioactive nature. Several studies indicate that biological waste materials can serve as calcium sources for hydroxyapatite synthesis, with eggshells being one such promising source. In the present work, two types of hydroxyapatite were synthesized: pure hydroxyapatite and 5% magnesium-doped hydroxyapatite (based on weight percentage). Laboratory-grade calcium hydroxide was used for synthetic HAp, while eggshell powder was employed for eggshell-derived HAp. The activity of the developed materials in biological environment was assessed using in vitro methods. Porous ceramic blocks were fabricated by compacting the powders using a hydraulic press and sintering them at 950°C. Powder samples calcined at 800°C were analysed by X-ray diffraction (XRD) to assess the lattice parameters and functional groups identification was done by Fourier transform infrared spectroscopy (FTIR) to identify. Apparent porosity was determined using Archimedes' principle, confirming the presence of pores in the pellets. Hemolysis studies demonstrated that the synthesized materials are hemocompatible. Simulated body fluid (SBF) studies confirmed the appearance of apatite layer on the sintered pellets, establishing the bioactive and interactive nature of the developed materials.

Keyword: Hydroxyapatite, eggshell waste, lattice parameter, surface morphology, in vitro biocompatibility

***Author for Correspondence**
Sourav Debnath

[1]Principal, Department of Mechanical Engineering, Central Tool Room and Training Center, Kolkata, West Bengal, India
[2]Associate Professor, Department of Biomedical Engineering, Netaji Subhash Engineering College, Kolkata, West Bengal, India
[3]Assistant Professor, Department of Electrical Engineering, Brainware University, Barasat, Kolkata, West Bengal, India
[4]Assistant Professor, Department of Metallurgical Engineering, Kazi Nazrul University, Asansol, Paschim Bardhaman, West Bengal, India

Received Date: March 15, 2026
Accepted Date: March 31, 2026
Published Date: May 05, 2026

Citation: Subhasis Nath, Sujan Krishna Samanta, Sourav Debnath, Soumya Mukherjee. Fabrication and Comparative Study of Synthetic and Eggshell Waste Derived Hydroxyapatite-Based Composites for Biomedical Applications. Journal of Polymer & Composites. 2026; 14(3): S33–S46p.

INTRODUCTION

The idea of "waste to health" is changing modern materials science by turning discarded biological and industrial by-products [1, 2], into useful resources for making materials that help society [3]. As waste generation increases worldwide, especially biomedical waste, researchers are working to turn these waste streams into valuable biomaterials. This approach helps solve both environmental and healthcare problems. Many studies have looked at using waste materials like bones, shells, eggshells, agricultural leftovers [4], and plant fibers as sustainable sources for making composites [5, 6] ceramics, and bioactive substances used in engineering and medicine.

Human bone is composed of a complex combination of organic and inorganic constituents, in which calcium hydroxyapatite $Ca_{10}(PO_4)6(OH)_2$

crystals are embedded within an organic collagen fiber matrix [7–9]. Over the years, researchers have employed various methods to synthesize hydroxyapatite, including wet chemical precipitation [10], mechanochemical processing [11], sol–gel techniques [12], solid-state methods [13], microwave irradiation [14], and hydrothermal routes [15]. Hydroxyapatite has received substantial attention in orthopedic and dentistry due to its numerous advantages. However, it possesses certain inherent limitations, such as brittleness [16] and a lack of osteoinductive properties. Ongoing research efforts aim to improve the mechanical strength and biological functionality of hydroxyapatite through various strategies, one of which involves the incorporation of mineral ions. Natural bone contains several mineral ions, including sodium, magnesium, zinc, iron, and carbonate. Several studies have shown these ions play a crucial role in the osseointegration process [17].

Among these ions, magnesium has gained significant importance due to its function in promoting osteogenic cell proliferation [18]. Bigi et al. [19] observed the effect of magnesium ions on hydroxyapatite. Landi et al. [20] described that magnesium plays a substantial role in the primary stages of bone osteogenesis and enhances bone growth. Kolmaset al. [21] highlighted the suitability of magnesium ions for implant fixation within host bone, attributing this effect to their influence on solubility, morphology, dissolution rate, and mechanical properties. E. Landi et al. [22] showed that the inclusion of magnesium ions into the hydroxyapatite lattice does not significantly alter its hexagonal apatitic structure, while effectively modifying its solubility. Yajing et al. [23] reported the cellular response of mouse calvarial cells to bothHAp and Mg-doped HAp coatings, and informed that addition didn't produce any adverse effects; instead, Mg-HAp coatings promoted early osteogenic activity in preosteoblasts. Serre et al. [24] used collagen–apatite composite sponges and observed that, at physiological pH, the presence of magnesium enhanced bone mineralization. Mehrjoo et al. [25] reported that Mg-HAp powders increased alkaline phosphatase activity, gene expression, and cell proliferation in MG-63 human osteoblastic cells. Jones et al. [26] demonstrated that magnesium incorporation increased calcification levels in mice. Furthermore, Landi et al. [27] compared the osteogenic performance of Mg-doped HAp and pure HAp granules implanted in the femoral region of rabbits and concluded that magnesium-containing specimens exhibited superior osteogenic effects.

In laboratory conditions, hydroxyapatite can be synthesized using calcium hydroxide. Several studies have also reported that hydroxyapatite can be prepared from biowaste generated through various human activities. Such biowastes contain trace elements such as Na^{+}, Zn^{2+}, and Mg^{2+} [28,29], which closely mimic the elemental composition of human bone and can be transformed into valuable bioproducts. Ruksudjarit et al. [30] developed nanocrystalline hydroxyapatite from bovine bone using a vibration-assisted milling process. Many researchers [31–33] have investigated camel and horse bones to identify their mineral constituents. In these studies, the bones were calcined at 700 °C for 2 h, resulting in the formation of nanosized hydroxyapatite along with the presence of various trace elements. Hydroxyapatite has also been extracted from pig bones through calcination at temperatures of 600°C, 800°C, and 1000°C [34, 35], producing rod-shaped, non-stoichiometric biological apatites. Pal et al. [36] synthesized hydroxyapatite from a biogenic source, namely fish scales, and conducted a detailed analysis of its physical characteristics. Murugan et al. [37] suggested that hydroxyapatite synthesized from different sources exhibits significant variations due to differences in preparation conditions and key constituent materials. Wen-Fu Ho et al. [38] successfully synthesized calcium phosphate bioceramics from eggshells using a solid-state method. Similarly, Yawei Shi et al. [39] produced porous carbon materials from eggshell waste, while Laurent et al. [40] investigated bone healing in maxillofacial surgery using powdered hen eggshells and reported excellent biocompatibility without any adverse effects. In India, a large quantity of eggshell waste is generated annually, which can be effectively utilized as a biomaterial for bone tissue repair [41]. In the present report, hydroxyapatite and magnesium-doped hydroxyapatite were synthesized from eggshells and compared in vitro with chemically synthesized hydroxyapatite samples.

EXPERIMENTAL METHODS

Preparation of Synthetic HAp, Egg Shell HAp and Composite Materials

Discarded eggshells were collected from various sources, including kitchens, canteens, and restaurants. The collected shells were thoroughly rinsed several times with tap water to remove adhered debris, followed by boiling at 100°C for 30–45 minutes. The cleaned shells were then dried in an oven (SICCO, Kolkata,Hot air dryer) for 4–5 hours. Subsequently, the dried shells were calcined at 800°C in a muffle furnace at a heating rate of 5°C/min. The calcined eggshells were ball-milled and sieved to obtain a fine powder. The resulting superfine eggshell powder was gradually dispersed in hot water. A stoichiometric amount of orthophosphoric acid (0.6 M) was mixed dropwise into the suspension under continuous stirring using a stirrer, while maintaining the pH between 11 and 12. After complete mixing, the precipitate was allowed to age for a day long in a cool, dark environment. The resulting semi-solid precipitate was then dried in an oven for approximately 48 hours and subsequently calcined at 800°C.

Synthetic hydroxyapatite (referred to in this work as pure HAp) was prepared using laboratory-grade calcium hydroxide and orthophosphoric acid following a similar procedure. Magnesium oxide was used as the dopant material, and a 5 % magnesium substitution was employed for the eggshell-derived hydroxyapatite.

Sample Preparation and Physical Characterization

The agglomerated and calcined ceramic lumps were triturated in a ball mill for 2–3 hours to get a fine ceramic powder. The resulting powder was compressed into cylindrical molds to form pellets by applying a pressure of 2 tons for a duration of 120 seconds using a pressing machine (Make: PEECO ,India). The pellets had specifications of 12 ± 0.05 mm in diameter and 5 ± 0.05 mm in thickness. The green density of each compacted sample was calculated. The pellets were then sintered at 950°C, after which the sintered density was measured.

Apparent Porosity

Porous ceramic samples play a significant role in implant applications, as bone tissue can be securely fixed and can grow through the interconnected pores. Porosity was calculated using Archimedes' principle. The apparent porosity (ϕ) was determined using the following relation:

Percentage apparent porosity $=[(W_a - W_d)/(W_a - W_i)]\times 100$
Where ,W_d= dry weight of sample.
W_i= weight of sample in water.
W_a= sample weight after removal from the water

XRD, FTIR Analysis

We performed an XRD study to calculate the lattice parameters of the developed powders. The study was done by a X-Ray diffractometer (Bruker, Japan). A scanning range of 20-60° was done.The resulting diffraction profile was thoroughly studied to identify the peaks for hydroxyapatire phases and any other secondary phases which may be there due to the presence of trace elements in the raw material. The lattice parameters were then calculated using the standard unit cell plane-spacing relationship to evaluate structural changes caused by ion incorporation or processing conditions.

The lattice parameters were calculated using the unit cell plane-spacing relationship [42].

$$\frac{1}{d^2} = \frac{4}{3}\left(\frac{h^2+hk+k^2}{a^2}\right)+\frac{l^2}{c^2}$$

Here, d represents the interplanar spacing between adjacent planes corresponding to a given set of Miller indices (h k l). The unit cell volume (V) was calculated using the relation $V = 0.866\ a^2c$ [36]. The crystallinity (Xc) of the developed ceramic samples was determined using the following equation:

$$X_C = \left(1 - \frac{V_{112/300}}{I_{300}}\right)$$

Where, the intensity of the hollow between the planes (112) and (300) reflections are taken as V112/300 and I300 is the intensity of (300) reflection ,The crystallite size of the samples was calculated by Scherrer's equation:D=0.9 λ/βcosθ[36] D= crystal size, λ=wavelength of X-ray ,β=broadening of diffraction line at half of its maximum intensity in radians, θ = angle of diffraction. The presence of functional group was confirmed through FTIR analysis ("Perkin-Elmer-1615, US") in the wavelength range of 500-4000 cm-1.

The relative intensity variation between the (112) and (300) diffraction planes was evaluated using the parameter $V_{112/300}$, where I_{300}represents the peak intensity corresponding to the (300) reflection. The average crystallite size of the samples was determined using Scherrer's equation:

$$D = \frac{0.9\lambda}{\beta \cos\theta}$$

where Ddenotes the crystallite size, λis the wavelength of the incident X-ray radiation, βis the full width at half maximum (FWHM) of the selected diffraction peak (in radians), and θis the Bragg diffraction angle. This method provides an estimate of the coherent diffraction domain size and is widely employed to evaluate structural characteristics in nanocrystalline materials.

The presence and nature of functional groups in the synthesized samples were examined using Fourier Transform Infrared (FTIR) spectroscopy (Perkin-Elmer 1615, USA) over a spectral range of 500–4000 cm^{-1}. The FTIR spectra were analyzed to confirm characteristic vibrational modes associated with chemical bonding and surface functionalities, thereby supporting structural and compositional interpretations obtained from XRD measurements.

Mechanical Testing

To function effectively in vivo, compacted porous materials must maintain mechanical integrity under physiological pressures at the implantation site. In this study, we evaluated the specimens' mechanical behavior by measuring hardness using a Vickers microhardness tester (Model VM 50, Instr. &Engg., India). The diamond pyramidal indenter creates a square impression, with an angle of 136° between opposite faces and 22° between the indenter face and the sample surface.

The Vickers hardness number (HV) is found by dividing the applied load (F) by the surface area of the indentation (A). In practice, A is calculated from the average diagonal length (d) of the mark. HV shows how well the material resists local plastic deformation and is given in gigapascals (GPa).

SEM AND EDAX Analysis

Surface morphology was studied by scanning electron microscopy (SEM)and the elemental composition was done by Energy-dispersive X-ray analysis (EDAX) of the compacted pellet samples. These analyses were used to study grain size, pore size, and crystal arrangement. The sintered hydroxyapatite and magnesium-doped hydroxyapatite pellets were fractured and examined using a SEM (Model JSM-5200, Tokyo, Japan). SEM images obtained at different magnifications provided insight into the microstructural features of the HAp samples and their doped counterparts after sintering at high temperatures. The presence and distribution of constituent elements were confirmed through EDAX analysis.

SBF Study

Bioresorption studies were conducted to evaluate the dissolution behavior of the sintered samples in a laboratory-prepared simulated body fluid (SBF) solution following the Kokubo method [43], while maintaining physiological pH at 7.4. The prepared samples were immersed in the SBF solution, which was renewed every three days. The experiment was carried out for a duration of one month. Apatite layer formation on the pellet surfaces was analyzed using scanning electron microscopy (SEM).

Bactericidal Study

The antimicrobial activity of the prepared samples was evaluated using nutrient agar medium inoculated with Staphylococcus aureus. The nutrient agar medium was sterilized by autoclaving at 121 °C for 20 minutes in a conical flask and then allowed to cool to approximately 40–45 °C. The cooled medium was inoculated with the Staphylococcus aureus culture and mixed thoroughly before being poured into Petri dishes. Porcelain discs containing the sample powder solution were then placed onto the agar surface and incubated at 35 °C for 24 hours. Two different sample concentrations, 3 mg/10 mL and 1 mg/10 mL, were used for the antimicrobial assessment.

MTT Assay

In the MTT assay, peripheral blood mononuclear cells (PBMCs) were used to assess cell viability. The cells were seeded in 24-well plates at a density of 5×1045 \times 10^45×104 cells/cm². The samples along with the cells were transferred into tubes and incubated for 24 hours. Subsequently, MTT solution (3-(4,5-dimethylthiazol-2-yl)-2,5-diphenyltetrazolium bromide) was added with gentle shaking for 15 minutes, followed by further incubation for 3–4 hours. After incubation, dimethyl sulfoxide (DMSO) was added to dissolve the formed formazan crystals, resulting in a purple-colored solution. The optical density was measured at 545 nm against a blank. The experiment was performed in triplicate, and the average value was reported.

Hemolysis Study

The hemolysis experiment was performed following the procedures outlined in the ASTM standard [44]. Human blood was collected and immediately mixed with a 3.8% sodium citrate solution in a 10:1 ratio to prevent coagulation. The anticoagulated blood was then further diluted using normal saline at a proportion of 4:5. For testing, 10 mL of normal saline was added to separate test tubes, and the prepared sample pellets were placed into these tubes and maintained at 37°C for 30 minutes. After this initial incubation, 0.2 mL of the diluted blood was introduced into each tube, followed by an additional one-hour incubation period.

In the positive control setup, normal saline was replaced with 10 mL of a 0.1% sodium carbonate solution, to which 0.2 mL of the diluted blood was added and incubated for one hour. The negative control consisted of 10 mL of normal saline mixed with 0.2 mL of diluted blood. All samples, including controls, were kept at 37°C for one hour and subsequently centrifuged at 500 g for five minutes. The supernatants were then collected, and their absorbance values were measured at 545 nm using a UV–Vis spectrophotometer (Elico India, SL-177).

The percentage of hemolysis is calculated from the following equation:

$$\%\text{Haemolysis} = \frac{\text{O.D(Test)} - \text{O.D(Negative)}}{\text{O.D (Positive)} - \text{O.D.(Negative.)}} \times 100$$

RESULTS AND DISCUSSION

Physical Properties

The experimented data are tabulated below in Table 1.

Table 1. Physical Properties.

Specimen	Hardness (GPa)	Avg.GreenDensity (g/cm^3)	Avg.Sintered Density (g/cm^3)	Apparent porosity (%)	pore size distribution (μm)
Pure HAp	3.63±0.032	1.52±0.021	2.96±0.016	21.02±1.56	14-167
Egg shell HAp	3.70±0.022	1.536±0.012	2.95±0.012	31.48±1.691	22-185
Pure HAp+Mg5%	3.68±0.017	1.574±0.016	3.02±0.015	24.31±2.38	18-177
Egg shell HAp+Mg5%	3.83±0.021	1.568±0.022	2.98±0.036	35.90±1.0	22-200

The results showed that magnesium-doped samples exhibited a higher percentage of porosity compared to the other samples. This increase in porosity may be attributed to the difference in atomic diameters between calcium and magnesium. Additionally, the eggshell-derived hydroxyapatite samples showed greater porosity, which may be due to the presence of residual impurities in the eggshell constituents. The measured hardness values indicate that the prepared samples possess sufficient mechanical strength to withstand stresses at the implant–tissue interface. Moreover, the observed porosity in all sintered samples was adequate to support a favorable biogenic environment for new tissue ingrowth and stable fixation.

XRD Study

The XRD patterns (Figure 1) exhibited characteristic diffraction peaks corresponding to the (002), (211), (202), (300), (212), and (222) planes, confirming the presence of crystalline hydroxyapatite in the prepared samples. These diffraction planes were indexed in accordance with the standard reference card JCPDS No. 09-0432. The peak intensities of pure HAp and eggshell-derived HAp were nearly identical, whereas slight peak shifts were observed in the magnesium-doped samples. The XRD patterns of pure HAp, eggshell-derived HAp, and their respective doped variants are presented in the Figure below.

The calculated lattice parameters revealed a reduction in both the *a* and *c* axes in the magnesium-doped samples. This decrease can be attributed to the substitution of calcium ions (atomic radius ≈ 197 pm) with smaller magnesium ions (atomic radius ≈ 160 pm) within the crystal lattice. The smaller ionic radius of magnesium is likely responsible for the observed lattice contraction. The results summarized in Table 2 confirm the successful substitution of calcium by magnesium ions and the corresponding reduction in unit cell dimensions. Crystalline percentage is decreased with incorporating magnesium into hydroxyapatite matrix.

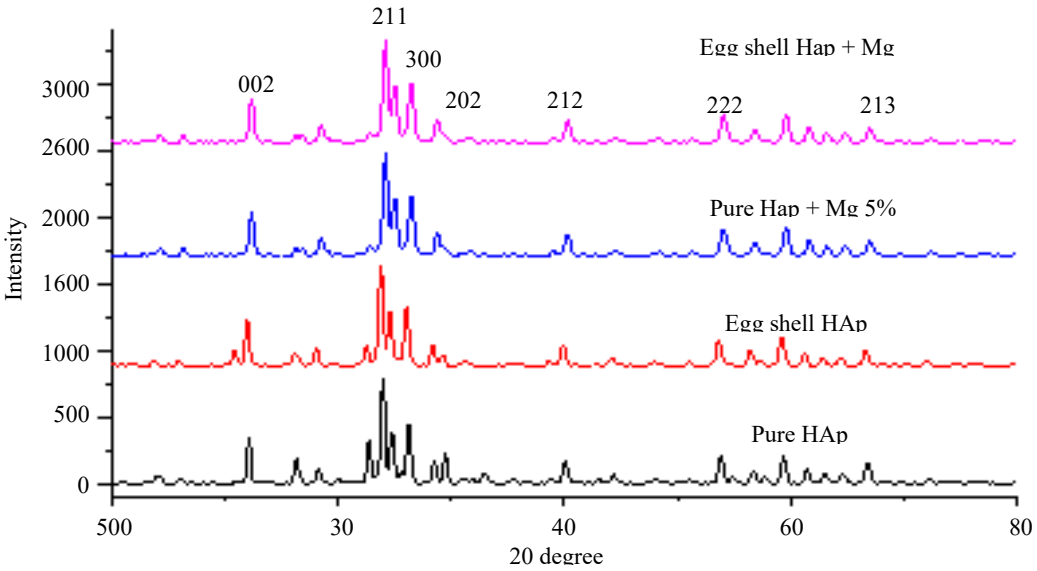

Figure 1. XRD of pure HAp, eggshell HAp and dopants.

Table 2. Lattice parameter.

Parameters	Pure HAp	Eggshell HAp	Pure Hap + 5% Mg	EggshellHAp + 5% Mg
a-axis(Å)	9.4130±0.0877	9.397±0.10	9.3030±0.086	9.311±0.492
c axis (Å)	6.741 ±0.121	6.687±0.16	6.541 ±0.121	6.526±0.27
Unit cell volume (Å3)	532.93±22.01	520.05±18.29	514.78±22.54	496.06±18.29
Crystallite size (Å)	3.6186±12.55	3.5456±9.84	3.3281±11.57	3.2821±14.77
% Crystallinity	93.71± 3.79	84.72±5.76	84.31± 4.11	82.02±5.76

FTIR Analysis

Figure 2 presents the FTIR spectra for pure hydroxyapatite, eggshell-derived hydroxyapatite, and their corresponding 5% magnesium-doped composites. All samples exhibited characteristic vibrational bands associated with the phosphate (PO_4^{3-}) groups, which are the primary structural units of hydroxyapatite. The prominent absorption peaks detected at approximately 562 cm^{-1} correspond to the O–P–O bending vibrations of the phosphate group, while the peak near 1016 cm^{-1} represents the P–O symmetric and asymmetric stretching modes. The presence of these well-defined phosphate bands confirms the formation of hydroxyapatite as the dominant crystalline phase in both the synthetic and biogenic samples.

Additionally, a distinct absorption peak at around 3744 cm^{-1} was observed, corresponding to the stretching vibration of the hydroxyl (OH^-) group, a signature feature of stoichiometric hydroxyapatite. The appearance of this peak indicates proper incorporation of hydroxyl ions within the apatite lattice and further validates the structural integrity of the synthesized materials.Minor variations in peak intensity and sharpness among the samples may be attributed to differences in crystallinity and microstructural characteristics arising from the use of eggshell precursors and magnesium substitution. The FTIR spectra confirm that all synthesized powders retain the characteristic functional groups of crystalline hydroxyapatite, with no evidence of secondary phases.

SEM and EDX Study

The scanning electron microscopy images (Figure 3) revealed the presence of pores within the sample materials, indicating that the prepared samples possessed sufficient porosity, which is essential for bone tissue ingrowth. Energy-dispersive X-ray analysis (EDAX) confirmed the presence of calcium, phosphorus, and magnesium ions in the corresponding samples as shown in Figure 4.

SBF Study

Bioactivity was clearly seen during the simulated body fluid (SBF) immersion study. After seven days, an initial apatite layer started to form on the surfaces of the sintered pellets. This early layer is typical for bioactive calcium phosphate materials and shows that the hydroxyapatite-based samples can interact well with the physiological ions in the SBF solution.

As the immersion period increased, more apatite was deposited. The surface became more covered, and the apatite layer looked denser and more evenly spread, showing that calcium-phosphate phases kept forming over time as shown in Figure 5.

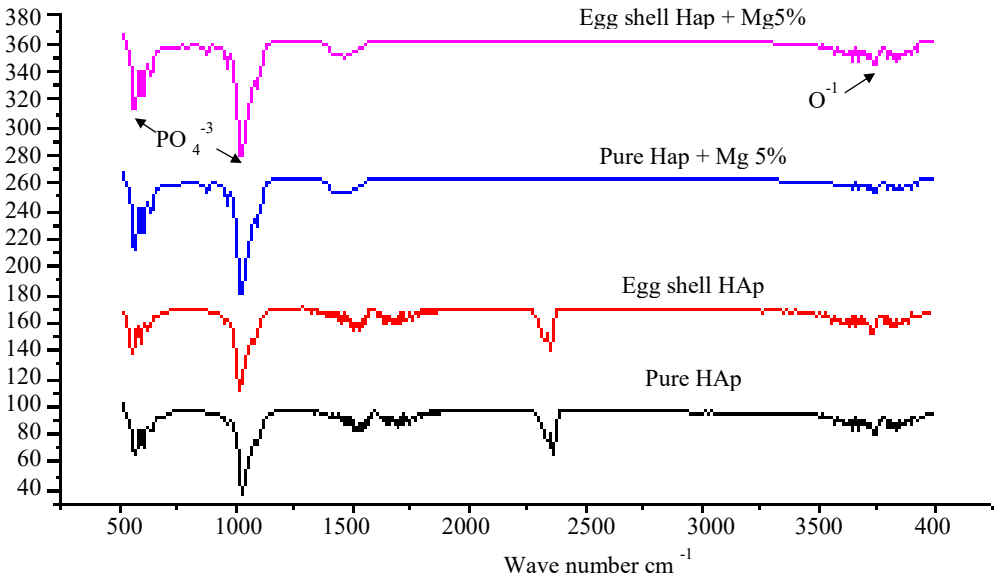

Figure 2. FTIR of pure HAp, eggshell Hap and their dopants.

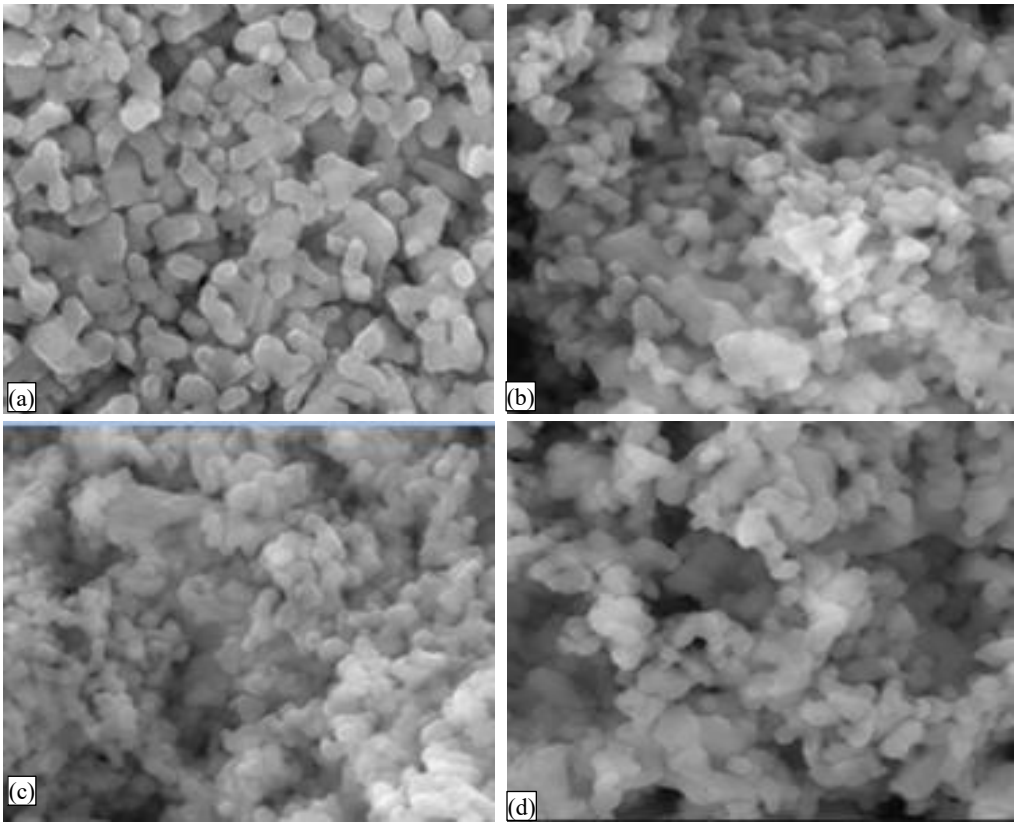

Figure 3. SEM picture of pure HAp, egg shell waste derived HAp and HAp based composites. (a) Pure Hap; (b) Egg shell Hap; (c) Pure Hap +mg 5%; (d) Egg shell Hap +mg 5%

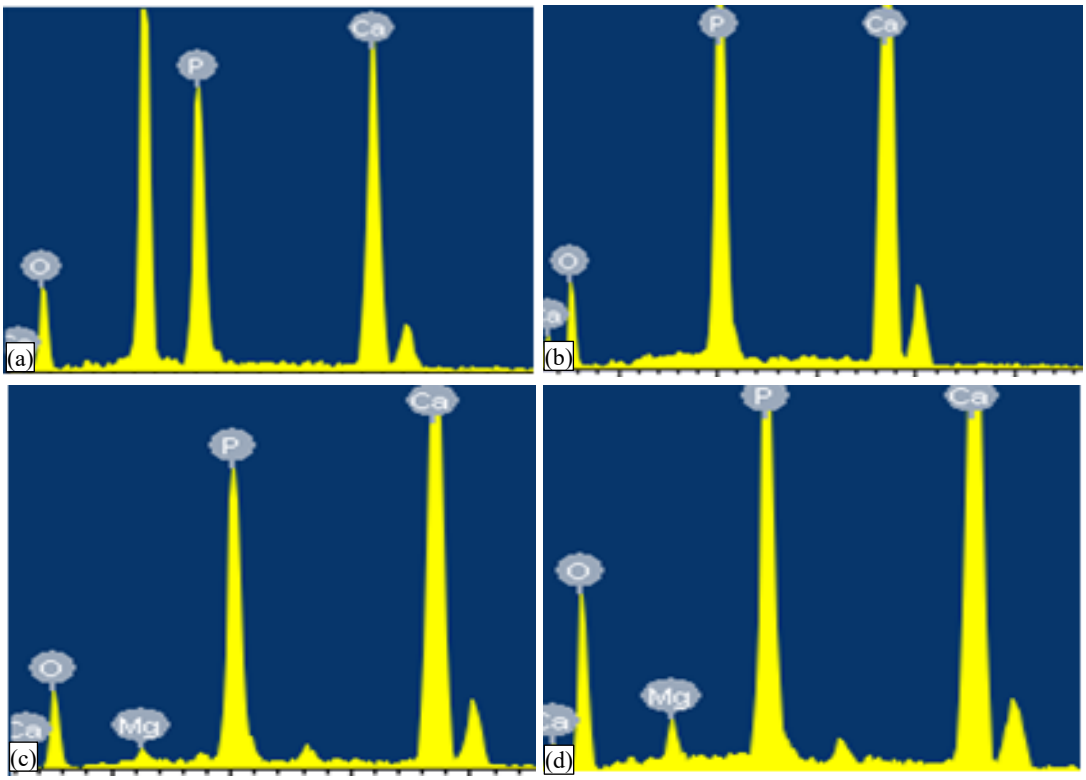

Figure 4. EDAX of pure HAp, eggshell waste derived HAp and HAp based composites. (a) Pure Hap; (b) Egg shell Hap; (c) Pure Hap +mg 5%; (d) Egg shell Hap +mg 5%

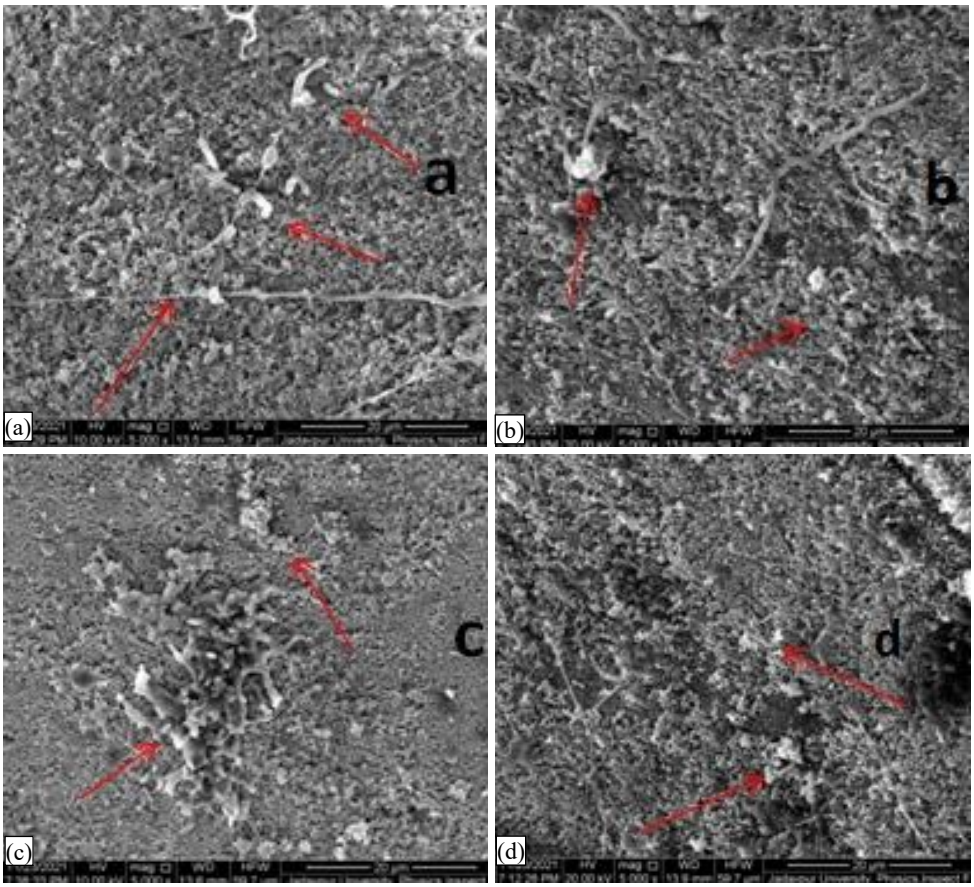

Figure 5. Apatite images of (a) Pure Hap; (b) Egg shell Hap; (c) 5% Mg- HApcomposite; (d) 5 % Mg-Egg shell HAp composite

This gradual thickening suggests the samples had strong ion-exchange activity, allowing them to take up Ca^{2+} and PO_4^{3-} ions from the SBF. This process is important for bonding the material to tissue in the body.

The steady growth of the apatite layer confirms that the hydroxyapatite and magnesium-doped hydroxyapatite samples have good osteoconductive potential. In such a study, ongoing apatite formation is taken as a sign that a material can form a stable bond with natural bone after implantation. So, the greater apatite buildup over time shows that these composites have the right surface reactivity for bone repair and regeneration.

Bactericidal and MTT Assay Study

The antimicrobial assessment revealed that none of the samples produced a visible zone of inhibition around the porcelain discs after 24 hours of incubation against *Staphylococcus aureus*. This absence of inhibition zones at both tested concentrations (3 mg/10 mL and 1 mg/10 mL) indicates that the synthesized hydroxyapatite and magnesium-doped hydroxyapatite materials do not possess inherent bactericidal or bacteriostatic properties under the tested conditions as shown in Figure 6. Although the samples did not demonstrate antimicrobial activity, their biological safety was confirmed through the MTT cytotoxicity assay. The bar diagram in Figure 7 shows that all tested samples maintained more than 80% cell viability, well above the threshold typically used to indicate cytocompatibility. This high percentage of viable cells suggests that neither the synthetic nor the eggshell-derived hydroxyapatite samples exerted toxic effects on peripheral blood mononuclear cells (PBMCs). Thus, despite the lack of bactericidal action, the materials are non-toxic and biocompatible, supporting their suitability for biomedical applications where safe interaction with host tissues is essential.

Red arrow and yellow arrow show the samples' concentration in porcelain bit of 3 mg/10ml and 1mg/10ml, respectively). No zone of inhibition was observed in any of the Petri dishes after 24 hours of incubation. The results indicated that the samples at both tested concentrations (3 mg/10 mL and 1 mg/10 mL) did not exhibit bactericidal activity.

The bar diagram representing the MTT assay (Figure 7) showed that all samples maintained more than 80% cell viability.

Hemolysis Study

Analysis of the hemolysis bar diagram (Figure 8) data showed that all the prepared samples exhibited less than 5% hemolysis. According to ASTM guidelines, this indicates that all the samples are hemocompatible.

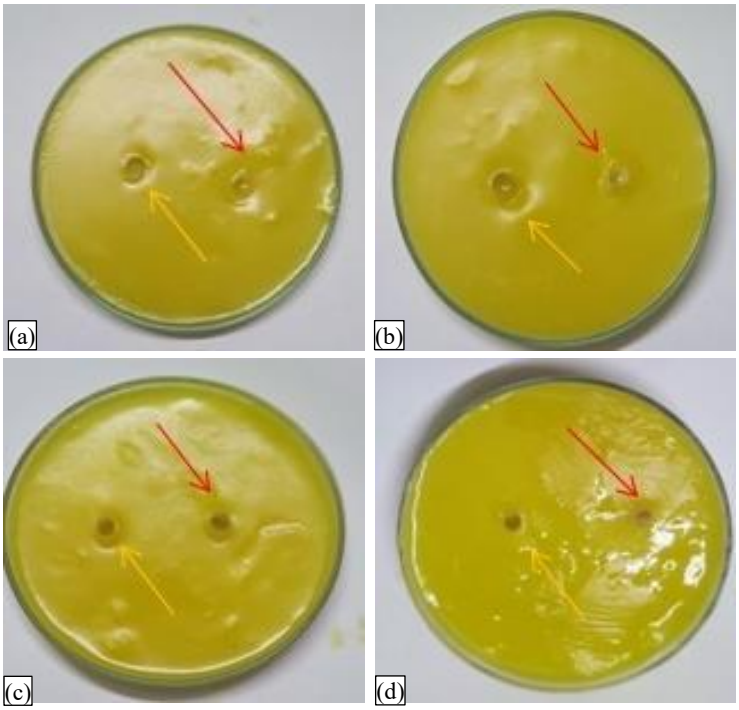

Figure 6. Petri dishes showing bactericidal images of pure HAp, egg shell Hap and HAp based composites. (a) Pure Hap; (b) Egg shell Hap; (c) Pure Hap +mg 5%; (d) Egg shell Hap +mg 5%

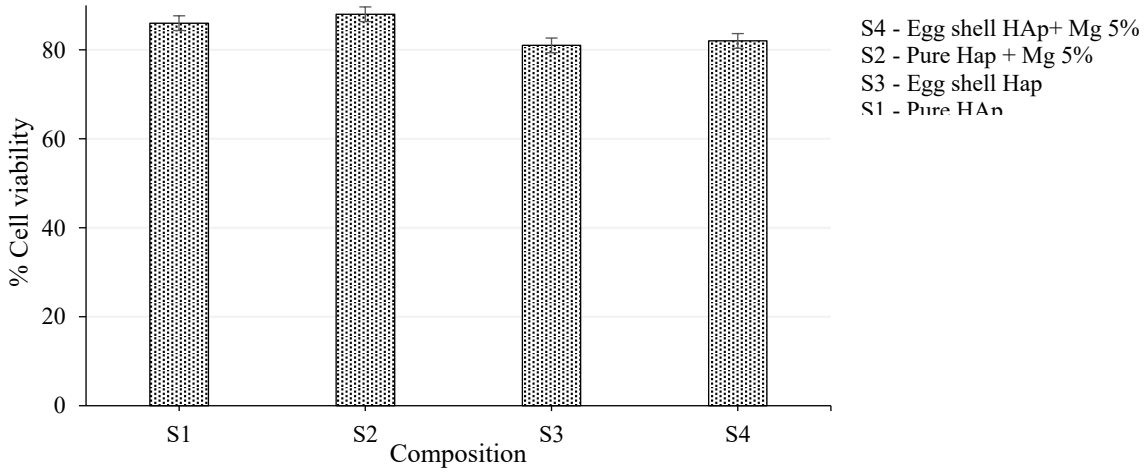

Figure 7. Bar diagram showing percent cell viability of samples.

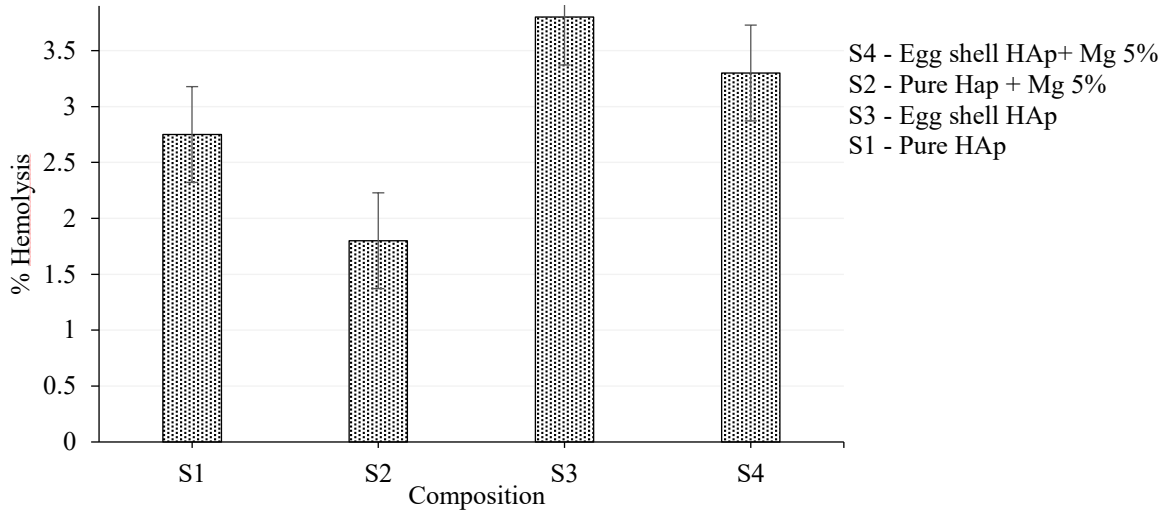

Figure 8. Diagrammatic representation of hemolysis (%).

CONCLUSION

In this study, magnesium-doped hydroxyapatite composites were successfully synthesized using both synthetic precursors and eggshell waste as calcium sources. Lattice parameter evaluation revealed distinct crystallographic modifications, particularly lattice contraction, confirming the successful incorporation of magnesium ions into the hydroxyapatite matrix. XRD analysis verified the formation of phase-pure hydroxyapatite in all samples, with diffraction peaks closely matching the standard JCPDS card No. 09-0432. Complementary FTIR and EDAX analyses further confirmed the presence of characteristic functional groups and constituent elements, validating the chemical integrity of the synthesized materials.

Microstructural assessment through SEM imaging, supported by apparent porosity measurements, demonstrated the presence of interconnected pores essential for cell infiltration and osteointegration. The bioactive nature of the materials was evidenced by the formation of apatite layers on sample surfaces during SBF immersion, indicating favorable osteogenic potential. In addition, cytocompatibility, hemocompatibility, and antimicrobial assessments collectively confirmed that all synthesized materials are biocompatible and safe for potential biomedical applications.Comparative evaluation between the two material sources revealed that eggshell-derived magnesium-doped hydroxyapatite exhibited slightly enhanced performance in terms of porosity, bioactivity, and overall biological interaction. These findings highlight eggshell waste as a sustainable, cost-effective, and efficient alternative precursor for producing functional hydroxyapatite-based bioceramics. The results provide a promising foundation for further exploration of biowaste-derived hydroxyapatite in orthopedic and dental implant applications.

AUTHOR CONTRIBUTIONS

The first author and the second author contributed equally to this work and share first authorship.

REFERENCES

1. Ayrilmis N, Kanat G, Yildiz Avsar E, Palanisamy S, Ashori A. Utilizing waste manhole covers and fibreboard as reinforcing fillers for thermoplastic composites. Journal of Reinforced Plastics and Composites. 2025;44(17–18):1108-1118. doi:10.1177/07316844241238507
2. Bhuvaneshwaran Mylsamy, Karthik Aruchamy, Senthil Kumar Marudhamuthu Shanmugam, Sivasubramanian Palanisamy, Nadir Ayrilmis, “Improving performance of composites: Natural and synthetic fibre hybridisation techniques in composite materials – A review,” Materials Chemistry

and Physics, Volume 334, 1 April 2025, 130439. https://doi.org/10.1016/j.matchemphys.2025.130439
3. Murugesan Palaniappan, Sivasubramanian Palanisamy, Thulasi mani Murugesan, Srinivas Tadepalli, Rashid Khan, Sabbah Ataya, Influence of Washing with Sodium Lauryl Sulphate (SLS) Surfactant on Different Properties of Ramie Fibres, BioResources, 19(2), 2609-2625, 2024. DOI: 10.15376/biores.19.2.2609-2625
4. Karuppusamy Manickaraj, Ramakrishnan Thirumalaisamy, Sivasubramanian Palanisamy, Nadir Ayrilmis, Ehab El Sayed Massoud, Murugesan Palaniappan, S. Lakshmi Sankar, Value-added utilization of agricultural wastes in biocomposite production: Characteristics and applications, Ann NY Acad Sci., 1549, 72–91, 2025. https://doi.org/10.1111/nyas.15368
5. Sivasubramanian Palanisamy, Mayandi Kalimuthu, Shanmugam Dharmalingam, Azeez Alavudeen, Rajini Nagarajan, Sikiru Oluwarotimi Ismail, Suchart Siengchin, Faruq Mohammad and Hamad A, Al-Lohedan6Effects of fiber loadings and lengths on mechanical properties of Sansevieria Cylindrica fiber reinforced natural rubber biocomposites, Materials Research Express, Mater. Res. Express 10 (2023) 085503, pp. 2-13, 2023. https://doi.org/10.1088/2053-1591/acefb0
6. Rajkumar Ramasubbu, Arumugam Kayambu, Sivasubramanian Palanisamy, and Nadir Ayrilmis, Mechanical Properties of Epoxy Composites Reinforced with Areca catechu Fibers Containing Silicon Carbide, BioResources 19(2), 2353–2370, 2024. DOI: 10.15376/biores.19.2.2353-2370
7. J. Henkel, M.A. Woodruff, D.R. Epari, R. Steck, V. Glatt, I.C. DIckinson, P.F.M. Choong, M.A. Schuetz, Di.W. Hutmacher, Bone Regeneration Based on Tissue Engineering Conceptions-A 21st Century Perspective, Bone Research. 1 (2013) 216–248. https://doi.org/10.4248/BR201303002.
8. T.S.B. Narasaraju, D.E. Phebe, Some physico-chemical aspects of hydroxylapatite, Journal of Materials Science. 31 (1996) 1–21. https://doi.org/10.1007/BF00355120.
9. J.F. Shackelford, Bioceramics - current status and future trends, Materials Science Forum. 293 (1999) 99–106. https://doi.org/10.4028/www.scientific.net/msf.293.99.
10. M.H. Santos, M. de Oliveira, L.P. de F. Souza, H.S. Mansur, W.L. Vasconcelos, Synthesis control and characterization of hydroxyapatite prepared by wet precipitation process, Materials Research. 7 (2004) 625–630. https://doi.org/10.1590/s1516-14392004000400017.
11. B. Nasiri-Tabrizi, P. Honarmandi, R. Ebrahimi-Kahrizsangi, P. Honarmandi, Synthesis of nanosize single-crystal hydroxyapatite via mechanochemical method, Materials Letters. 63 (2009) 543–546. https://doi.org/10.1016/j.matlet.2008.11.030.
12. A.Borello, A. Deptuła, W. Łada, T. Olczak, C. Alvani, A. Di Bartolomeo, NON-CRYSTALLINE SOLIDS Preparation of spherical powders of hydroxyapatite, Journal of Non-Crystalline Solids. 148 (1992) 537–541.
13. S. Pramanik, A.K. Agarwal, K.N. Rai, A. Garg, Development of high strength hydroxyapatite by solid-state-sintering process, Ceramics International. 33 (2007) 419–426. https://doi.org/10.1016/j.ceramint.2005.10.025.
14. T.S. Sampath Kumar, I. Manjubala, J. Gunasekaran, Synthesis of carbonated calcium phosphate ceramics using microwave irradiation, Biomaterials. 21 (2000) 1623–1629. https://doi.org/10.1016/S0142-9612(00)00014-4.
15. H.S. Liu, T.S. Chin, L.S. Lai, S.Y. Chiu, K.H. Chung, C.S. Chang, M.T. Lui, Hydroxyapatite synthesized by a simplified hydrothermal method, Ceramics International. 23 (1997) 19–25. https://doi.org/10.1016/0272-8842(95)00135-2.
16. T.J. Webster, E.A. Massa-Schlueter, J.L. Smith, E.B. Slamovich, Osteoblast response to hydroxyapatite doped with divalent and trivalent cations, Biomaterials. 25 (2004) 2111–2121. https://doi.org/10.1016/j.biomaterials.2003.09.001.
17. N. Murugan, C. Murugan, A.K. Sundramoorthy, In vitro and in vivo characterization of mineralized hydroxyapatite/polycaprolactone-graphene oxide based bioactive multifunctional coating on Ti alloy for bone implant applications, Arabian Journal of Chemistry. 11 (2018) 959–969. https://doi.org/10.1016/j.arabjc.2018.03.020.

18. Cacciotti, A. Bianco, M. Lombardi, L. Montanaro, Mg-substituted hydroxyapatite nanopowders: Synthesis, thermal stability and sintering behaviour, Journal of the European Ceramic Society. 29 (2009) 2969–2978. https://doi.org/10.1016/j.jeurceramsoc.2009.04.038.
19. A. Bigi, G. Falini, E. Foresti, A. Ripamonti, M. Gazzano, N. Roveri, Magnesium influence on hydroxyapatite crystallization, Journal of Inorganic Biochemistry. 49 (1993) 69–78. https://doi.org/10.1016/0162-0134(93)80049-F.
20. E. Landi, A. Tampieri, M. Mattioli-Belmonte, G. Celotti, M. Sandri, A. Gigante, P. Fava, G. Biagini, Biomimetic Mg- and Mg,CO3-substituted hydroxyapatites: synthesis characterization and in vitro behaviour, Journal of the European Ceramic Society. 26 (2006) 2593–2601. https://doi.org/10.1016/j.jeurceramsoc.2005.06.040.
21. J. Kolmas, A. Jaklewicz, A. Zima, M. Bućko, Z. Paszkiewicz, J. Lis, A. Ślósarczyk, W. Kolodziejski, Incorporation of carbonate and magnesium ions into synthetic hydroxyapatite: The effect on physicochemical properties, Journal of Molecular Structure. 987 (2011) 40–50. https://doi.org/10.1016/j.molstruc.2010.11.058.
22. E. Landi, A. Tampieri, G. Celotti, S. Sprio, Densification behaviour and mechanisms of synthetic hydroxyapatites, Journal of the European Ceramic Society. 20 (2000) 2377–2387. https://doi.org/10.1016/S0955-2219(00)00154-0.
23. Y. Yajing, D. Qiongqiong, H. Yong, S. Han, X. Pang, Magnesium substituted hydroxyapatite coating on titanium with nanotublar TiO 2 intermediate layer via electrochemical deposition, Applied Surface Science. 305 (2014) 77–85. https://doi.org/10.1016/j.apsusc.2014.02.163.
24. C.M. Serre, M. Papillard, P. Chavassieux, J.C. Voegel, G. Boivin, Influence of magnesium substitution on a collagen–apatite biomaterial on the production of a calcifying matrix by human osteoblasts., Journal of Biomedical Materials Research. 42 (1998) 626–633. https://doi.org/10.1002/(sici)1097-4636(19981215)42:4<626::aid-jbm20>3.3.co;2-j.
25. M. Mehrjoo, J. Javadpour, M. Ali Shokrgozar, M. Farokhi, S. Javadian, S. Bonakdar, Effect of magnesium substitution on structural and biological properties of synthetic hydroxyapatite powder, Materials Express. 5 (2015) 41–48. https://doi.org/10.1166/mex.2015.1205.
26. J.E. Jones, R. Schwartz, L. Krook, Calcium homeostasis and bone pathology in magnesium deficient rats, Calcified Tissue International. 31 (1980) 231–238. https://doi.org/10.1007/BF02407186.
27. E. Landi, G. Logroscino, L. Proietti, A. Tampieri, M. Sandri, S. Sprio, Biomimetic Mg-substituted hydroxyapatite: From synthesis to in vivo behaviour, Journal of Materials Science: Materials in Medicine. 19 (2008) 239–247. https://doi.org/10.1007/s10856-006-0032-y.
28. D. Milovac, T.C. Gamboa-Martínez, M. Ivankovic, G. Gallego Ferrer, H. Ivankovic, PCL-coated hydroxyapatite scaffold derived from cuttlefish bone: In vitro cell culture studies, Materials Science and Engineering C. 42 (2014) 264–272. https://doi.org/10.1016/j.msec.2014.05.034.
29. M. Akram, R. Ahmed, I. Shakir, W.A.W. Ibrahim, R. Hussain, Extracting hydroxyapatite and its precursors from natural resources, Journal of Materials Science. 49 (2014) 1461–1475. https://doi.org/10.1007/s10853-013-7864-x.
30. A. Ruksudjarit, K. Pengpat, G. Rujijanagul, T. Tunkasiri, Synthesis and characterization of nanocrystalline hydroxyapatite from natural bovine bone, Current Applied Physics. 8 (2008) 270–272. https://doi.org/10.1016/j.cap.2007.10.076.
31. J. Sang Cho, S.H. Um, D. Su Yoo, Y.C. Chung, S. Hye Chung, J.C. Lee, S.H. Rhee, Enhanced osteoconductivity of sodium-substituted hydroxyapatite by system instability, Journal of Biomedical Materials Research - Part B Applied Biomaterials. 102 (2014) 1046–1062. https://doi.org/10.1002/jbm.b.33087.
32. S.S. Rahavi, O. Ghaderi, A. Monshi, M.H. Fathi, A comparative study on physicochemical properties of hydroxyapatite powders derived from natural and synthetic sources, Russian Journal of Non-Ferrous Metals. 58 (2017) 276–286. https://doi.org/10.3103/S1067821217030178.
33. H.L. Jaber, A.S. Hammood, N. Parvin, Synthesis and characterization of hydroxyapatite powder from natural Camelus bone, Journal of the Australian Ceramic Society. 54 (2018) 1–10. https://doi.org/10.1007/s41779-017-0120-0.

34. A.M. Janus, M. Faryna, K. Haberko, A. Rakowska, T. Panz, Chemical and microstructural characterization of natural hydroxyapatite derived from pig bones, Microchimica Acta. 161 (2008) 349–353. https://doi.org/10.1007/s00604-007-0864-2.
35. E.A. Ofudje, A. Rajendran, A.I. Adeogun, M.A. Idowu, S.O. Kareem, D.K. Pattanayak, Synthesis of organic derived hydroxyapatite scaffold from pig bone waste for tissue engineering applications, Advanced Powder Technology. 29 (2018) 1–8. https://doi.org/10.1016/j.apt.2017.09.008.
36. A. Pal, S. Paul, A.R. Choudhury, V.K. Balla, M. Das, A. Sinha, Synthesis of hydroxyapatite from Lates calcarifer fish bone for biomedical applications, Materials Letters. 203 (2017) 89–92. https://doi.org/10.1016/j.matlet.2017.05.103.
37. R. Murugan, S. Ramakrishna, Crystallographic study of hydroxyapatite bioceramics derived from various sources, Crystal Growth and Design. 5 (2005) 111–112. https://doi.org/10.1021/cg034227s.
38. W.F. Ho, H.C. Hsu, S.K. Hsu, C.W. Hung, S.C. Wu, Calcium phosphate bioceramics synthesized from eggshell powders through a solid state reaction, Ceramics International. 39 (2013) 6467–6473. https://doi.org/10.1016/j.ceramint.2013.01.076.
39. Y. Shi, H. Ke, J. Xie, H. Tan, G. Luo, B. Xu, G. Abakari, Jo u pr oo f, Geoderma Regional. (2020) e00484. https://doi.org/10.1016/j.algal.2023.103165.
40. L. Dupoirieux, D. Pourquier, F. Souyris, Powdered eggshell: a pilot study on a new bone substitute for use in maxillofacial surgery, Journal of Cranio-Maxillofacial Surgery. 23 (1995) 187–194. https://doi.org/10.1016/S1010-5182(05)80009-5.
41. S. Sasikumar, R. Vijayaraghavan, Low temperature synthesis of nanocrystalline hydroxyapatite from egg shells by combustion method, Trends in Biomaterials and Artificial Organs. 19 (2006) 70–73.
42. Anushika, P. Sharma, A. Trivedi, H. Begam, Synthesis and characterization of pure and titania doped hydroxyapatite, Materials Today: Proceedings. 16 (2019) 302–307. https://doi.org/10.1016/j.matpr.2019.05.094.
43. T. Kokubo, H. Takadama, How useful is SBF in predicting in vivo bone bioactivity?, Biomaterials. 27 (2006) 2907–2915. https://doi.org/10.1016/j.biomaterials.2006.01.017.
44. ASTM F 756-00, Standard practice for assessment of hemolytic properties of materials. Philadelphia, American Society for Testing and Materials. (2000) 5. https://doi.org/10.1520/F0756-13.

